Hydrol. Earth Syst. Sci. Discuss., 10, 15337–15373, 2013
www.hydrol-earth-syst-sci-discuss.net/10/15337/2013/
doi:10.5194/hessd-10-15337-2013

Hydrology and Earth System Sciences
Open Access
Discussions

Effects of land-conversion in a biosphere–atmosphere model of Northern South America – Part 2: Case studies on the mechanisms of differential hydrometeorology

R. G. Knox[1,*], M. Longo[2], A. L. S. Swann[3], K. Zhang[2], N. M. Levine[2], P. R. Moorcroft[2], and R. L. Bras[4]

[1]Massachusetts Institute of Technology, Cambridge, Massachusetts, USA
[2]Harvard University, Cambridge, Massachusetts, USA
[3]University of Washington, Seattle, Washington, USA
[4]Georgia Institute of Technology, Atlanta, Georgia, USA
[*]now at: Lawrence Berkeley National Laboratory, Berkeley, California, USA

Received: 22 October 2013 – Accepted: 17 November 2013 – Published: 13 December 2013

Correspondence to: R. G. Knox (rgknox@lbl.gov)

Published by Copernicus Publications on behalf of the European Geosciences Union.

Abstract

A physical model of the terrestrial biosphere (Ecosystem Demography Model) is combined with an atmospheric model (Brazilian Regional Atmospheric Modeling System) to investigate how land conversion in the Amazon and Northern South America have changed the hydrology of the region. Two numerical realizations of the structure and composition of terrestrial vegetation are used as boundary conditions in a simulation of the regional land surface and atmosphere. One realization seeks to capture the present day vegetation condition that includes human deforestation and land-conversion, the other is an estimate of the potential structure and composition of the region without human influence. Two focus areas, one in the Brazilian state of Pará, and one in the Bolivian Chaco, are selected to scrutinize the basis of differential hydrology and hydrometeorology manifested by the two scenarios. In both cases, deforestation led to increases in total surface albedo, driving decreases in net-radiation, boundary layer moist static energy and ultimately convective precipitation. In the case of the Bolivian Chaco, decreased precipitation was also a result of decreased advective moisture transport, indicating that differences in local hydrometeorology may manifest via teleconnections with the greater region.

1 Introduction

There are several direct hydrologic mechanisms that connect tropical forests (or the lack thereof) to the regional climate system. Stems and leaves absorb light at different magnitudes over the visible and thermal spectrum compared to bare earth and grasses, typically resulting in a lower surface albedo and higher levels of net surface radiation. This directly impacts atmospheric radiative heating/cooling rates and the net flux of sensible and latent heat into the atmosphere. Forest leaf surfaces also increase the interception of precipitation, which influences the land surface water balance and the partition that is re-directed toward the atmosphere. Forests typically have higher leaf

HESSD
10, 15337–15373, 2013

areas and therefore higher total capacity for transpiration due to higher total stomata density.

Forests also draw from deeper soil moisture pools, which have different periodicity in available water and therefore alter the timing of latent heat flux via transpiration compared to grasslands (Kleidon and Heimann, 2000; Nepstad et al., 1994). Below the canopy crown, litter-fall and forest floor vegetation combine with leaf interception to enhance overall retention of water from runoff both on the surface and through the soil matrix. Canopy structure also changes the drag surface imposed on the atmospheric boundary layer and the manifestation of shear and in-canopy turbulent transport of heat, moisture and momentum.

The differential effects that forests and non-forests have on surface hydrology, shift the balance of latent and sensible heat flux creating a potential trade-off between the mechanisms that trigger convective initiation and the mechanisms that sustain deep convection (Peilke, 2005; Wang et al., 2009). Latent heat flux is a potential source of convective available potential energy (CAPE) which is essential for driving deep convection. However, sensible heat flux drives the large thermal motions that stimulate boundary layer growth and are likewise needed to trigger convection (Pielke, 2001).

This article, in combination with it's companion paper, is interested in uncovering the local and regional scale sensitivities of hydrologic climate in response to present day land conversion in the Amazon and Northern South America. The first article described the design, validation and regional assessment of the differential hydrologic response of two coupled ecosystem-atmosphere simulations using the The Ecosystem Demography Model 2 (ED2) (Moorcroft et al., 2001; Medvigy, 2006) and the Brazilian Regional Atmospheric Model (BRAMS) (Cotton et al., 2003). To re-iterate, the two simulations are identical regarding time, space, physical parametrization and lateral boundary conditions, yet singularly differ regarding how the biosphere model (ED2) represents the structure (the distribution of plant sizes) and composition (the distribution of plant types) of the region's terrestrial ecosystems. In one simulation, the regional terrestrial vegetation elements in ED2 reflect a structure and composition that has no effects of human

HESSD
10, 15337–15373, 2013

land-use, i.e., a *Potential Vegetation* condition. In the other simulation, the ED2 model incorporates an estimate of modern (e.g., 2008) human land-use, i.e., an *Actual Vegetation* condition. This article steps away from the regional perspective of its companion, and focuses on the hydrology and hydrometeorology present in two focus areas.

2 Selection of case studies

The regional assessment of differences in annual precipitation from the companion paper identified two areas where model estimated annual precipitation were consistently different, significantly different, and occurred where the ecosystems showed moderate to strong water limitations to growth. The differences in precipitation at these two locations featured spatial dipoles, where one lobe had significant differential increases in precipitation and one lobe had significant decreases in precipitation. One dipole was near the Amazon delta with negative differential precipitation in northern Pará (i.e., precipitation in the human land-use scenario "AV" was less than the potential scenario "PV"). The other dipole was along the Andean foothills in eastern Bolivia, its negative differential over the Chaco region. Significance and consistency in precipitation and radiation was determined via standard scores and relative differences. Ecosystem susceptibility was determined by looking at the moisture stress index of the region's ecosystems (an explanation is described in the companion paper), these maps are provided again (see Fig. 1).

Two locations that coincide with the dipole precipitation lobes are highlighted in Fig. 1. Each location shows significant decreases in normalized precipitation and increases in down-welling short-wave radiation associated with the *Actual Vegetation* case. The vegetation of these locations also show varying degrees of moisture stress. Site 1 is centered on 4.5° S 50.5° W, site 2 is centered on 19.5° S 63.5° W. These sites will be explored in greater detail in the following sections.

HESSD
10, 15337–15373, 2013

3 Case study hydrology – site 1: Pará, 4.5° S 50.5° W

The case study in Pará Brazil can be described by significant deforestation and a negative (AV–PV) precipitation differential. The natural landscapes are dominated by tropical evergreen forests that receive on the order of 1.5 m of annual rainfall, and are close to (but not within) the ecotone transition between tropical forests and Cerrado. Pastures account for an estimated 1/3 of the land-cover. Roughly 10% of the landscape contains old-growth forests over 200 yr old. See Fig. 2 for a profile of the model estimated vegetation structure and composition.

The site of interest is modeled by a single ED2 polygon. A model polygon contains within it a distribution of landscapes of variable disturbance history, each of which contain a distribution of vegetation cohorts which compete for light, water and carbon resources in a vertically distributed canopy air space. The precipitation at this site represents a differential (AV–PV) that is among the upper percentiles of sites in the area. Surface energy flux is dominated by leaf evaporation and transpiration. Transpiration dominates vapor flux in the dry season (May–November) when intercepted precipitation is minimized. Total runoff in the form of drainage occurs mostly during the wet season for PV forests. Figure 3 provides a time integration of the PV forest water balance and the differential water balance.

Leaf evaporation and transpiration decrease in the land-conversion scenario, which is consistent with decreases in precipitation. However the evaporated fraction of precipitation (Fig. 5) also decreases with land conversion, which is consistent with reduced stomatal and leaf surface density seen in deforestation.

This significant shift in evaporative fraction drives a cycle of mass balance changes. In human land-use scenario, even with less total precipitation the massive decrease in leaf evaporation drives a greater total volume of water reaching the surface. With more precipitation through-fall and less root zone uptake, the equilibrium soil moisture of converted lands increases and leads to greater runoff and greater soil evaporation. Once the water is exported from the system as runoff, it cannot return to moisten the canopy.

HESSD
10, 15337–15373, 2013

However the increased soil evaporation is also influenced by transport processes. Decreases in leaf evaporation and transpiration significantly decreases the cooling and moistening of the canopy air in deforested lands (see Fig. 4), driving increased vapor pressure gradients with the surface. Moreover, in these simulations, deforestation also reduces the mean regional surface drag and promotes greater above canopy wind-speeds. The EDM2 parameterizations use wind-speed to calculate shear and diffusivity at the top of the canopy, which governs the scale of the in-canopy diffusivity and vertical scalar flux.

The actual vegetation scenario (AV) receives more total short-wave and long-wave radiation ($R_{SD} + R_{LD}$), which is undoubtedly related to a decrease in mean convective cloud albedo associated with the decrease in convective rainfall at the site. Although the site receives more total incoming radiation in the AV scenario, the surface albedo decreases with the conversion of forests to pasture. This results in more reflected radiation and a decrease in combined sensible and latent heat flux ($H + L$), see the right panel of Fig. 5.

In summary, land conversion has promoted a modest decrease in mean annual rainfall on the order of 10 %. The (AV) scenarios canopies are warmer and drier, particularly in the late dry season (August–September), a symptom of decreased cooling from leaf evapotranspiration and the direct losses to latent canopy cooling. The warmer and drier canopies of the converted lands drive higher sensible heating rates. The higher surface temperatures of converted lands are in equilibrium with higher upwelling thermal radiation rates. The combination of increased thermal radiation and surface albedo result in lower mean net radiation in the converted scenario.

The dry-season precipitation experienced at this site is primarily convective, and therefore the differences experienced may be driven by differential surface energy flux associated with land-conversion. A focused evaluation of the atmosphere during September 2003 may elucidate these differences in precipitation and cloud albedo. A box is constructed in the area around this site, it bounds the depression in differential precipitation and evapotranspiration for the month (see Fig. 6).

HESSD
10, 15337–15373, 2013

Table 1 shows the mean results of the bounded domain. Results are spatially consistent with the single site time-series analysis. While there is more incident down-welling short-wave radiation at the converted lands, there is less net-radiative heating, likely attributed to increases surface albedo and emitted thermal radiation. The hotter surface temperatures at the converted lands are a symptom of decreased evaporative cooling. Both sites are losing energy at the surface (storage), which is associated with the loss of enthalpy through water mass in the canopy and soil layers.

The decreases in AV scenarios convective precipitation can be traced back to an analysis of instability and mechanical energy, mean profiles of equivalent potential temperature and turbulent kinetic energy at 12 a.m. (15Z model time) are provided in Fig. 7. The AV scenario has significantly less instability in terms of equivalent potential temperature, yet significantly more turbulent kinetic energy. The decreases in equivalent potential temperature is partially explained by local differences in total surface energy flux, the AV scenario has a monthly mean bias of $-10\,\mathrm{W\,m^{-2}}$. The convergence of moisture provides information regarding the non-local influence on precipitation. Both cases net a negative moisture convergence budget for the month. The PV scenario loses more precipitable water ($-51.32\,\mathrm{kg\,m^{-2}}$) through its lateral boundaries than the AV scenario ($-37.14\,\mathrm{kg\,m^{-2}}$), see Table 1.

The advective moisture flux is driven by a strong easterly flow (see Fig. 8). The right panel in Fig. 8 shows the differential flux vectors of precipitable water (AV–PV). The flow vectors run parallel to the coast in this dry season month, originating from areas with relatively lower mean precipitable water. The moisture flux vectors flow *up-gradient* along total column precipitable water, which is consistent with the total moisture divergence defining the bounded domain.

Boundary layer turbulent kinetic energy is essential in forming convective updrafts. When there is a layer of negative buoyancy between the top of the mixed layer and the level of free convection (where a surface parcel attains positive buoyancy with the environment), turbulent eddies provide the energy necessary for lifting moist surface parcels through negative buoyancy. In theory, increases in turbulent kinetic energy

HESSD
10, 15337–15373, 2013

could promote greater frequency of convective initiation. Given that the AV case experienced less total accumulated rainfall, this would possibly translate into a greater number of weak and possibly non-precipitating events. Histograms were constructed that tracked the key levels in *precipitating* convective events, including the level where updrafts originate (LOU), the lifting condensation level (LCL), level of free convection (LFC) and the level of neutral buoyancy (LNB) (see Fig. 9). The histograms indicate that despite having less boundary layer TKE, there were more precipitating events for the Potential Vegetation scenario.

A simple conceptual model of this system is to approximate the dynamics of the bounded region as fully and instantaneously mixed. With this assumption, the fraction of precipitation derived from water coming from surface evaporation is simply the ratio of evaporation over the combination of evaporation and lateral moisture convergence. With the fully and instantaneously mixed assumption, a region that is experiencing negative moisture convergence would therefore trace all precipitated water back to surface evaporation. In a divergent system, a perturbation in precipitation would be proportional to the perturbation in surface evaporation. Of course, a fully and instantaneously mixed model is a crude representation of reality. But it can be rationalized that convective plumes originate at the surface where evaporation feeds directly into the atmospheric boundary layer. That said, the lateral flux of moisture is continuously mixing with surface air through eddy motions, and moreover influences the atmospheric profiles that entrain and detrain with convective clouds.

The moisture flux at this location is divergent, the rainfall is convectively driven and the even though the potential vegetation simulation produces more precipitation it also experiences increased divergence. In other words, even though it has more moisture divergence, there is still more precipitation. This combination of factors supports the conclusion that differences in the surface energy flux is driving the differences in precipitation. And therefore, increased divergence of total precipitable water is a result of more out-flowing water vapor sedimenting into rainfall.

HESSD
10, 15337–15373, 2013

In summary, the the land-surface condition with deforestation (AV) had higher levels of sensible heat flux and more turbulent kinetic energy. Although, the difference was not strong enough to generate more convective events. A significant number of the updrafts from the (AV) simulation had overcome negative buoyancy but then lacked the moist static energy necessary generate precipitation and deep convection.

4 Case study hydrology – site 2: Chaco, 19.5° S 63.5° W

Site 2 is located in the Bolivian Gran Chaco, east of the foothills of the Andes mountains. This site is unique in that it is located in a region influenced by the outlet of the South American Low Level Jet. The continental precipitation recycling ratios in this area are generally very high (in our definition, meaning that most of the precipitation can be traced back to the continental land mass as opposed to the ocean). In the coupled simulation (AV case), precipitation in the area ranged from 500 to almost 1000 mm. Annual precipitation in the Potential Vegetation (PV) scenarios were typically higher, with biases upwards of 200 mm yr^{-1}. The vegetation profile (see Fig. 10), shows natural landscapes are grasslands with sparse cover of short tree canopies. The GLU land-use dataset (Hurtt et al., 2006) dictated 25 % of the landscape to pasture, with an accompanying 20 % of abandoned and degraded lands. Human land-use at this specific location promoted a complete collapse of the tree cover, which includes natural landscapes. This specific site is undoubtedly a more aggressive representation of the differences between the actual and potential ecosystems in this region. Human land-conversion of course, has not lead to a collapse of the Chaco's forest ecosystems for the region as a whole.

The cumulative water balance at this site features the hydrologic effects of decreased (AV) precipitation on the order of 15 % (see Fig. 11). This site is different than the Pará site in that the land-conversion scenario received less through-fall. Human land-conversion typically reduces the density of precipitation interception surfaces (leaves and stems), and would by direct response increase the through-fall fraction. At the

HESSD
10, 15337–15373, 2013

Bolivia site, the relative decrease in precipitation interception surfaces associated with land-conversion was proportionally less significant than the decrease in total precipitation incident on the canopy. As a result, even less precipitation reached the soil surface in the AV scenario. Regarding other key fluxes, soil evaporation is the dominant component of total water losses at the site. Leaf evaporation and transpiration contribute about 25 % of the total losses each, drainage is negligible in both cases.

There is a distinct difference in the moisture profiles between the two scenarios, the time series for each case is provided in Fig. 12. Despite the decreased net through-fall in the AV scenario, upper soil column moisture from rain events has a longer residence time in the root zone. This is an effect of decreased transpiration, and thus moisture in the grass root zone lasts comparatively longer into the dry season. However, soil surface evaporation rates are also higher in the (AV) scenario grass canopy. This promotes a comparatively more dessicated root zone and surface moisture state in the mid to late dry season. The AV scenario vegetation is completely grass and has a shallow rooting system, below 1.5 m there is no root uptake which promotes increased soil moisture in the lower column.

Depending on the strength of wet season precipitation, total moisture flux through the soil column (precipitation, transpiration, soil evaporation, drainage) eventually slowed down in the late dry season (August, September) for both cases. Little water exchange occurred with the canopy air over this period. This is conveyed in Fig. 13 which shows the net gains and losses of soil column moisture. It is clear that soil moisture losses are stronger in the PV scenario after rain events, where greater infiltration of water is more rapidly drawn up in the root zone by increased transpiration. The delayed dry-season losses are also clear for the AV scenario.

The simulation with land-conversion receive more incident radiation (short and long-wave) (see Fig. 14). This is an effect of decreased cloud albedo, associated with decreased activity of precipitating convective clouds. However, like the Pará site, land-conversion here also drives an increase in total surface albedo and surface long-wave radiation, which ultimately creates a condition of decreased net surface radiation (even

HESSD
10, 15337–15373, 2013

with less incident short-wave radiation). The relatively lower AV scenario latent heat flux is consistent with relatively lower total mean precipitation. The AV scenario soil-canopy system is dryer, which leads to proportionally more cooling through the release of sensible heat than latent heat. However the albedo effect on decreased net-radiation offsets the bowen ratio effect on sensible heat flux, the result is that sensible heat flux shows very little bias between the two scenarios.

In summary, both canopy incident precipitation and precipitation through-fall decreased in the AV scenario. The decrease in stomatal density at the AV site drove decreased transpiration, which enabled longer residence time in root zone soil moisture. Although, the soils eventually became even drier in the late dry season most likely due to increased exposure to radiative heating at turbulent transport at the soil surface. As with the Pará site, human land-conversion drove decreased net radiation due to surface albedo effects. From the meteorologic perspective, less energy is transfered back to the atmosphere with the presence of land-conversion.

April of 2003 features early dry-season hydrology with strong differences in precipitation between the two cases, this month is taken as a case study for the hydrometeorology of the immediate region (in the same fashion as the Pará site). A bounding box is constructed around the rough boundaries where a depression is experienced in differential precipitation (AV–PV), it is shown by a red line in Fig. 15.

Domain mean totals for change in precipitable water ΔM_{pw}, accumulated evapotranspiration ET, precipitation P and resolved moisture convergence Mc for the month of April are provided in Table 2. The PV scenario experiences over twice as much precipitation than the AV scenario (85 $kg\,m^{-2}$ compared to 41 $kg\,m^{-2}$). Differential evaporation between the two scenarios is not as extreme (111 $kg\,m^{-2}$ in the PV scenario compared to 83 $kg\,m^{-2}$ for AV). Along with a decrease in total precipitable water ΔM_{pw}, the domain showed negative moisture convergence in both cases, which is typical as April is the onset of the dry season in this region. The PV scenario showed significantly less moisture divergence (−37 $kg\,m^{-2}$) than the AV scenario (−52 $kg\,m^{-2}$). The land-surface storage of internal energy is decreasing over the month for both sites.

HESSD
10, 15337–15373, 2013

The increased divergence of moisture in the converted lands could be explained in various ways. Is it a symptom of less water advecting into the box, or more water advecting out of the box? It is clear that regional land-conversion has significantly influence the South American circulation. The moisture advected into this region comes via Northerly winds from the moist Amazonian air mass, see the left panel of Fig. 16. Moisture transport from the north decreases significantly in the AV scenario, see the right panel of Fig. 16.

The next consideration is how exactly does the differential precipitation in these two scenarios come to be at this location of interest. There is clearly more late morning instability in the potential vegetation scenario, equivalent potential temperature is significantly greater over the whole lower troposphere (see Fig. 17). There is very little differences in the profiles of turbulent kinetic energy. The higher monthly precipitation in the PV scenario is mostly attributed to the triggering of more convective events. This is evident in the records of mid-afternoon convective failures in the cumulus parameterization schemes for the two scenarios (see Fig. 18). This can be partially explained by the fact that more instances of convective initiation in the AV case failed to overcome negative buoyancy between the updraft base and the level of free convection, see flag 3. But this is the less significant mode of differences. The record also captured the number of events that were able to overcome buoyancy, but lacked the convective available potential energy to generate deep convection (flag 6).

In summary, this region showed reduced convective precipitation in the AV scenario due to both decreased ability to overcome negative buoyancy, and instances of weak convection upon achieving buoyancy. The inability to achieve deep convection was due to decreased moist static energy, particularly in the lower boundary layer (although the difference was significant across the lower troposphere). This is likely symptomatic of both a decrease in total and latent heat flux at the surface, and an overall decrease in advected precipitable water.

HESSD
10, 15337–15373, 2013

5 Conclusions

The fraction of rainfall that penetrates a vegetated canopy is a function of both the distribution of rainfall intensity and volume incident on the canopy as well as the state of the interception surfaces. Deforestation, which directly reduces leaf and stem interception surfaces, did not always translate into increased through-fall. The site at Chaco showed that decreases in precipitation associated with land-conversion could be significant enough to drive decreases in through-fall, even if leaf interception surfaces were decreased due to land-conversion.

The case studies also showed that the structure of the vegetation canopy influences the seasonal cycle of the moisture storage and vertical moisture flux of the canopy-soil system. At the Chaco site, transpiration was greater in the potential case during the wet season, due to increased root uptake and stomatal density. However, total evaporation was greater in the actual vegetation condition at the onset of the dry-season, due mostly to the fact that the grasslands had more available water still stored in the upper root-zone.

The (PV) vegetation at the Chaco site is generally described in model terms as open canopy early successional broad-leaf evergreens with accompanying C4 grasses. This region, as observed in the field, is renowned for the confluence of semi-arid, mountain, tropical and dry-forest ecotones. The biodiversity of the region supports a range of plants adapted to different competition schemes, most notably different water conservation and usage strategies. It must be realized that the range of water conservation strategies observed in nature could influence how the differences in surface to atmosphere energy fluxes play out at this site. The early successional competition strategy is fitting in dry forests to some extent, mostly in their ability to make opportunity out of a disturbance event. The southern Bolivian dry forests are indeed influenced by fire, and fitting for opportunists. But model vegetation parameters that are more closely associated with tropical vegetation may be adapted to shorter and less severe dry seasons. They may not regulate stomata in the late wet season or early dry season,

HESSD
10, 15337–15373, 2013

because the climate guarantees water will be available again soon. Plants that evolve in climates with short dry seasons are not going to benefit from regulating stomata in the dry season, it would be more advantageous for these plants to keep their stomata open in order to assimilate more carbon, be productive and more competitive for the limited available light. However, in the Chaco dry forests, plants are likely to have a different usage strategy for available root zone soil moisture.

The seasonal flux of surface to atmosphere water vapor (or the plants' regulation thereof), can potentially impact the hydrometeorological dynamic of the region. Total evapotranspiration during the transition from the late wet season to early dry season (April) at the Bolivian site was significantly larger in the potential vegetation scenario. The difference was strong enough that the increased moist static energy released by the land-surface stimulated enhanced deep convection (although it is thought that increased moisture flux from the tropical forests in the north was also a contributing factor). At this time, the differential transpiration rates of the two scenarios was a significant component of the difference. Therefore, the resource usage strategy of the deep rooted vegetation place an impact in the coupled dynamic of the system.

The precipitation regime of the site at Pará promoted a complete wetting of the soil column, this was not so for the case study at the Chaco site. As a result of increased total column water availability, the increased stomatal and root density of the potential scenario experienced greater differential uptake and transpiration through the dry season. As such, significant differential hydrometeorologic effects peaked in the mid to late dry-season mediated through differential transpiration. The precipitatoin regime at the Chaco did not have this complete wetting effect, and therefore the greatest differences were encountered earlier in the seasonal cycle as the wet season was completing.

It must be stated that the differential results of these simulations are undoubtedly influenced to some degree by the choices made in how the model is parameterized. For instance, the successful triggering of convection was based on the negative energy between the level of updraft (LOU) and the level of free convection (LFC). The LOU in our model framework is determined as the level in the planetary boundary layer with the

HESSD
10, 15337–15373, 2013

most turbulent kinetic energy. The LFC is determined by lifting a parcel from the LOU adiabatically until it matches density (and allowing for phase change) with the ambient atmosphere. The negative energy a parcel needs to overcome to reach the level of free convection is directly proportional to where its starting point (LOU) is decided, and boundary layer wind speeds impact this starting point. However, various levels of sophistication can be implemented as to how and if this layer of negative buoyancy is overcome by these air-parcels in the boundary layer.

In this experiment, we chose a parameterization that simply compares the negative buoyancy to a threshold value. Other triggering mechanisms may evaluate the distribution of vertical kinetic energy present in eddy motions at the LOU and estimate the likelihood of overcoming negative buoyancy through force balance computations. The message is that the effect of turbulence is mediated differently through these various choices, as it is in all physical parameterizations of the environment, and we must be mindful of this in our conclusions.

The negative precipitation bias associated with land-conversion at the two sites of interest, were attributed to significant decreases in boundary layer moist static energy and thus weaker convective events. Weak convection is typified by buoyant updrafts that lack the moist static energy to ascend several thousand meters. In deep convective events there is greater release of convective available potential energy and condensation of water vapor leading to increased rainfall. The decreases in moist static energy of AV scenario simulations were due to decreases in latent and total surface energy flux, brought on by decreases land surface albedo, leaf water interception and the ability to draw water from the lower soil column (which showed different seasonality according to the sites soil moisture flushing). In the case study at Pará, differences in precipitation were responding almost completely to localized differences in land-surface energy fluxes. The case study at the Bolivian Chaco suggests that human land-conversion has reduced the strength of the South American moisture circulation in the South Western portion of the Amazon, and that the reduction in this south-ward transport is equally

HESSD
10, 15337–15373, 2013

significant as land-surface differential energy fluxes in its influence over precipitation in the area.

Acknowledgements. This work was made possible through both the National Science Foundation Grant ATM-0449793 and National Aeronautics and Space Administration Grant NNG06GD63G. The authors would like to thank D. Entekhabi and E. A. B. Eltahir for their generous discussion and council.

References

Cotton, W., Pielke, R., Walko, R., Liston, G., Tremback, C., Jiang, H., McAnelly, R., Harrington, J., Nicholls, M., Carrio, G., and McFadden, J.: RAMS 2001: current status and future directions, Meteorol. Atmos. Phys., 82, 5–29, 2003. 15339

Hurtt, G. C., Frolking, S., Fearon, M. G., Moore, B., Shevialokova, E., Malyshev, S., Pacala, S. W., and Houghton, R. A.: The underpinnings of land-use history: three centuries of global gridded land-use transitions, wood harvest activity and resulting secondary lands, Global Change Biol., 12, 1–22, 2006. 15345

Kleidon, A. and Heimann, M.: Assessing the role of deep rooted vegetation in the climate system with model simulations: mechanism, comparison to observations and implications for amazonian deforestation, Clim. Dynam., 16, 183–199, 2000. 15339

Medvigy, D.: The State of the Regional Carbon Cycle: Results from a Constrained Coupled Ecosystem–Atmosphere Model, Ph.D. thesis, Harvard University, Cambridge, Massachusetts, USA, 2006. 15339

Moorcroft, P., Hurtt, G., and Pacala, S.: A method for scaling vegetation dynamics: the ecosystem demography model, Ecol. Monogr., 71, 557–586, 2001. 15339

Nepstad, D., de Carvalho, C., Davidson, E., Jipp, P., Lefebvre, P., Negreiros, H., dal Silva, E., Stone, T., Trubore, S., and Vieira, S.: The role of deep roots in the hydrological and carbon cycles of amazonian forests and pastures, Nature, 372, 666–669, 1994. 15339

Peilke, R.: Land use and climate change, Science, 310, 1625–1626, 2005. 15339

Pielke, R.: Influence of the spatial distribution of vegetation and soils on the prediction of cumulus convective rainfall, Rev. Geophys., 39, 151–171, 2001. 15339

HESSD

10, 15337–15373, 2013

Wang, J., Chagnon, F., Williams, E., Betts, A., Renno, N., Machado, L., Bisht, G., Knox, R., and Bras, R.: The impact of deforestation in the Amazon basin on cloud climatology, P. Natl. Acad. Sci. USA, 106, 3670–3674, 2009. 15339

HESSD
10, 15337–15373, 2013

Table 1. Hydrologic monthly means within the bounded area above case study 1, September 2003. Total change in column precipitable water ΔM_{pw}, evapotranspiration ET, precipitation P and resolved moisture convergence Mc, 55 m air temperature T, mixing ration (55 m) r, equivalent potential temperature θ_e, surface albedo to short-wave radiation α, down-welling short-wave radiation R_{SD}, down-welling long-wave radiation R_{LD}, up-welling long-wave radiation R_{LU}, net surface radiation R_{net}, sensible heat flux SHF and latent heat flux LHF.

Case	ΔM_{pw}	ET	P	Mc	T	r		
Units	$kg\,m^{-2}$	$kg\,m^{-2}$	$kg\,m^{-2}$	$kg\,m^{-2}$	°C	$g\,kg^{-1}$		
AV	−3.457	63.1	29.8	−37.14	32.83	12.18		
PV	−3.515	94.7	47.3	−51.32	32.35	12.93		
Case	θ_e	α	R_{SD}	R_{LD}	R_{LU}	R_{net}	SHF	LHF
Units	K	–	$W\,m^{-2}$	$W\,m^{-2}$	$W\,m^{-2}$	$W\,m^{-2}$	$W\,m^{-2}$	$W\,m^{-2}$
AV	336.8	0.262	300.2	443.3	513.2	180.9	139.25	70.97
PV	338.2	0.257	285.6	443.9	498.0	187.8	114.50	106.45

HESSD
10, 15337–15373, 2013

Table 2. Hydrologic monthly means within the bounded area above the Chaco case study (site 2), April 2003. Total change in column precipitable water ΔM_{pw}, evapotranspiration ET, precipitation P and resolved moisture convergence Mc, 55 m air temperature T, mixing ration (55 m) r, equivalent potential temperature θ_e, surface albedo to short-wave radiation α, down-welling short-wave radiation R_{SD}, down-welling long-wave radiation R_{LD}, up-welling long-wave radiation R_{LU}, net surface radiation R_{net}, sensible heat flux SHF and latent heat flux LHF.

Case	ΔM_{pw}	ET	P	Mc	T	r		
Units	$kg\,m^{-2}$	$kg\,m^{-2}$	$kg\,m^{-2}$	$kg\,m^{-2}$	°C	$g\,kg^{-1}$		
AV	−11.42	82.95	41.89	−52.49	25.98	12.73		
PV	−11.02	111.89	85.91	−36.99	27.36	15.15		
Case	θ_e	α	R_{SD}	R_{LD}	R_{LU}	R_{net}	SHF	LHF
Units	K	–	$W\,m^{-2}$	$W\,m^{-2}$	$W\,m^{-2}$	$W\,m^{-2}$	$W\,m^{-2}$	$W\,m^{-2}$
AV	334.4	0.330	252.6	400.2	466.9	111.74	38.54	91.0
PV	342.0	0.297	218.7	424.9	462.6	130.2	28.15	122.5

HESSD
10, 15337–15373, 2013

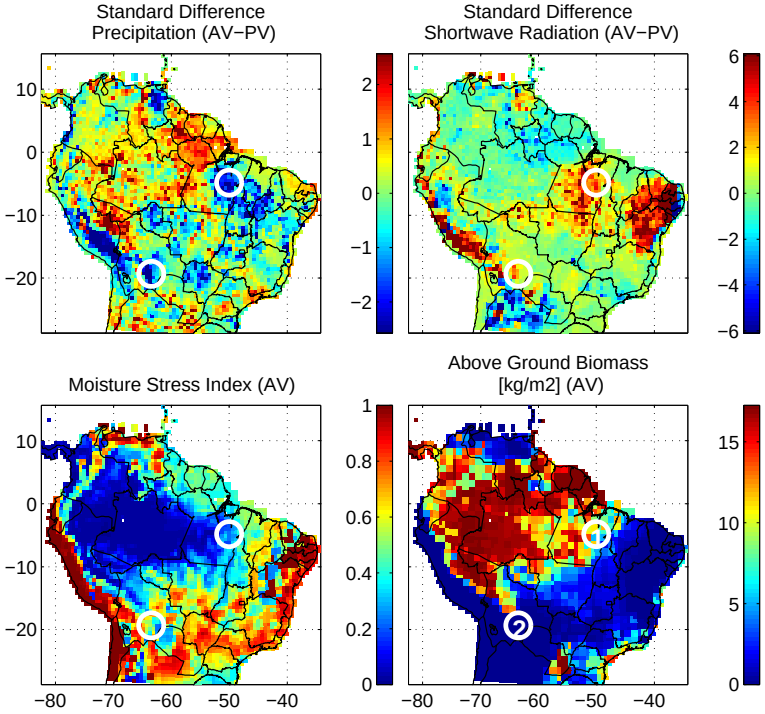

Fig. 1. Combined assessment of the regional significance in differences between precipitation and radiation, and the susceptibility of the ecosystems. Upper panels show standard scores reflecting surface precipitation and surface down-welling short-wave radiation. The lower left panel shows the moisture stress index for the (AV) scenario. For reference, (AV) scenario Above Ground Biomass is provide in the bottom right panel.

HESSD
10, 15337–15373, 2013

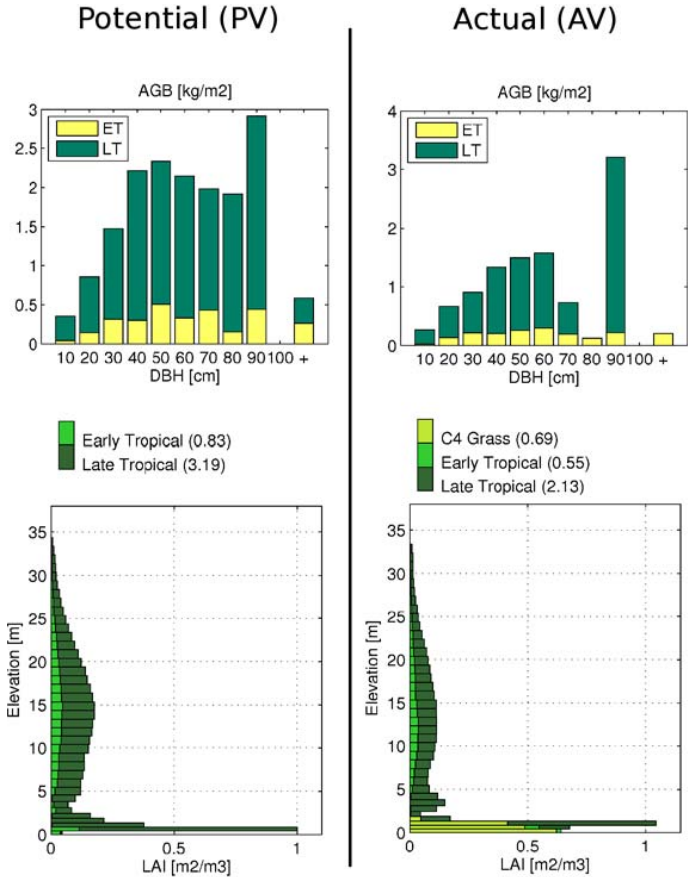

Fig. 2. Vegetation structure and composition estimated by the Ecosystem Demography Model 2 at Site 1 (4.5° S 50.5° W).

HESSD
10, 15337–15373, 2013

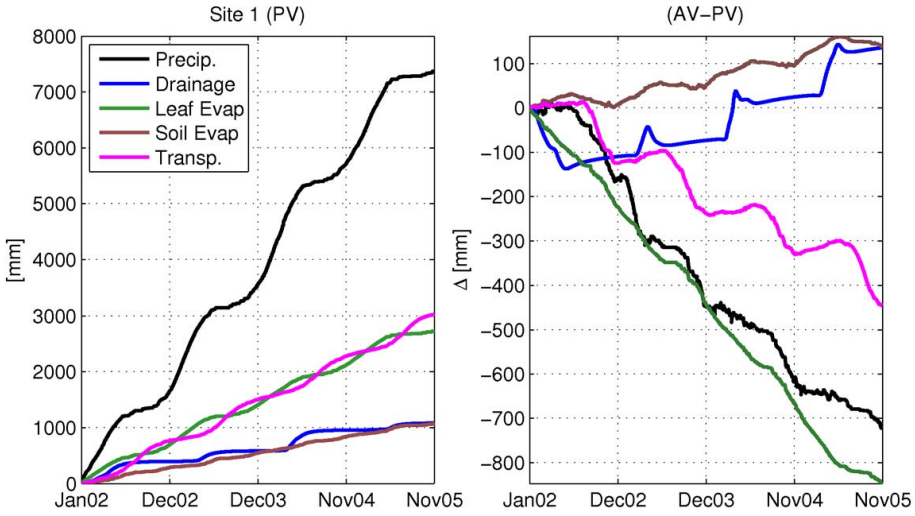

Fig. 3. Time series accumulations of water mass flux through the vegetation canopy at site 1 during the coupled model experiment, 2002–2005. The left panel shows accumulated fluxes in the PV case. Differences are shown in the right panel.

HESSD
10, 15337–15373, 2013

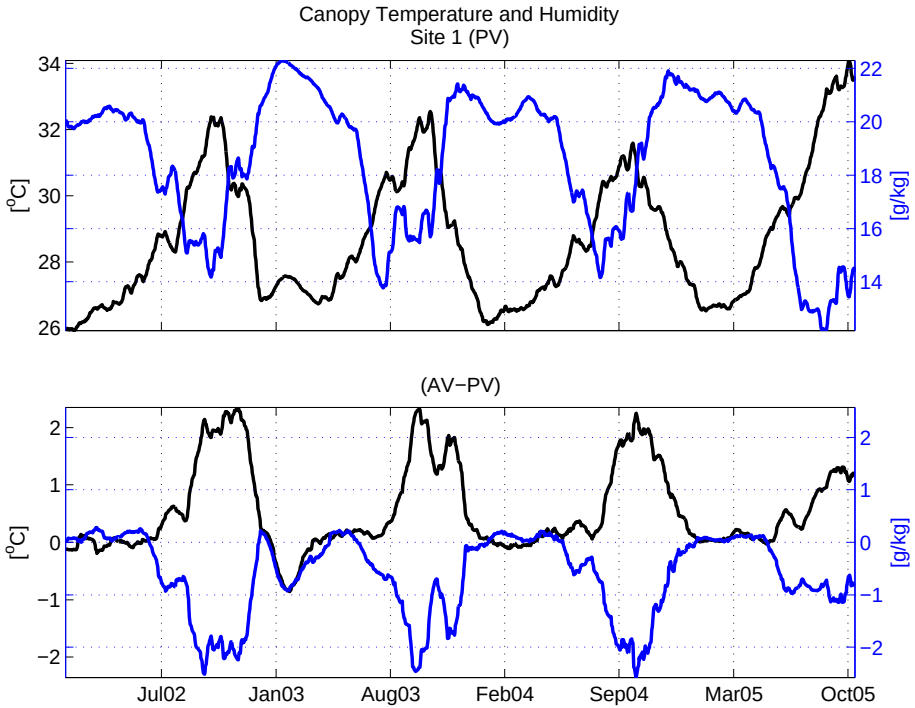

Fig. 4. Upper panel: time series of mean daily canopy temperature and humidity at site 1 during the coupled model experiment. Lower panel: differential canopy temperature and humidity.

HESSD
10, 15337–15373, 2013

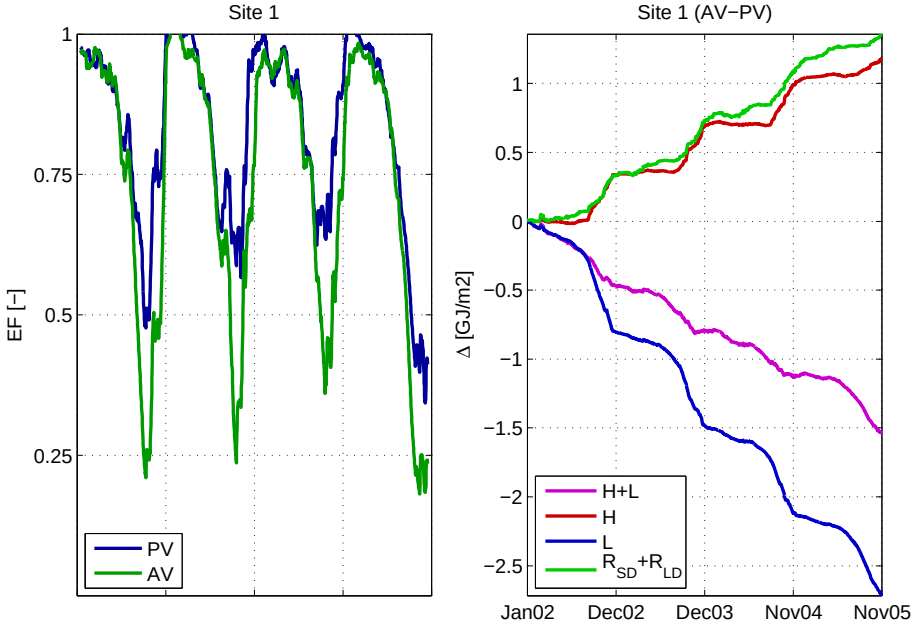

Fig. 5. Left panel: time series of evaporative fraction (latent/(latent+sensible)) at site 1. Right panel: time series of the differential in accumulated energy fluxes at site 1.

HESSD
10, 15337–15373, 2013

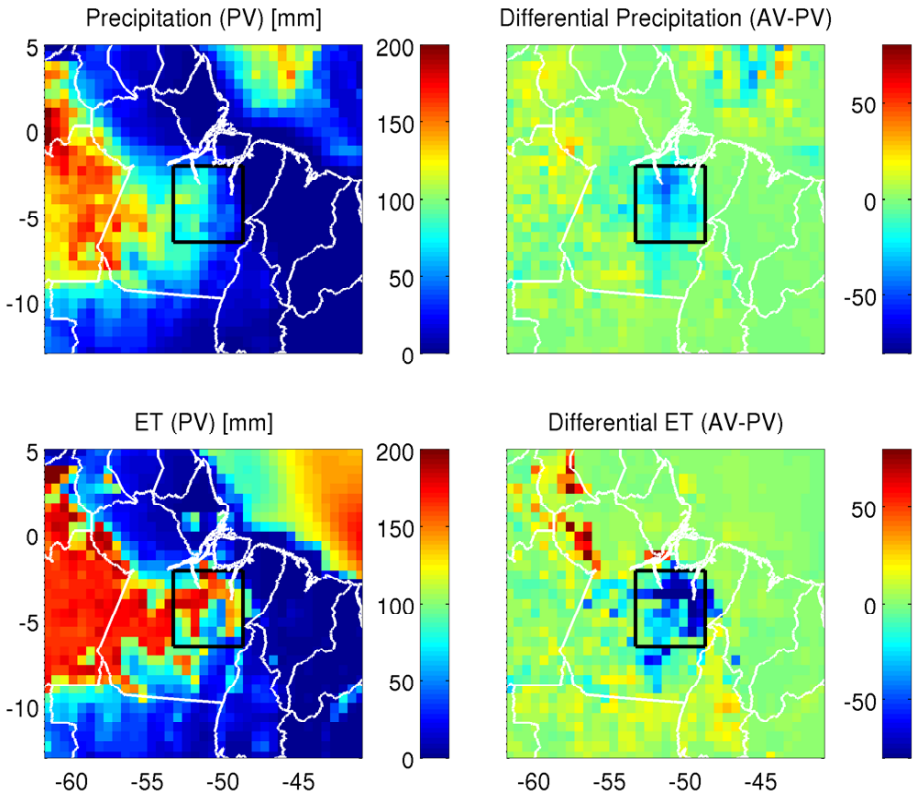

Fig. 6. Upper left panel: map of integrated monthly precipitation, case AV. Upper right panel: map of the integrated difference in monthly precipitation, case PV minus case AV. Lower right panel: map of integrated monthly evapotranspiration, case AV. Lower left panel: map of the integrated difference in monthly evapotranspiration, case PV minus case AV. The boundaries of the focus region are provided. September 2003.

HESSD
10, 15337–15373, 2013

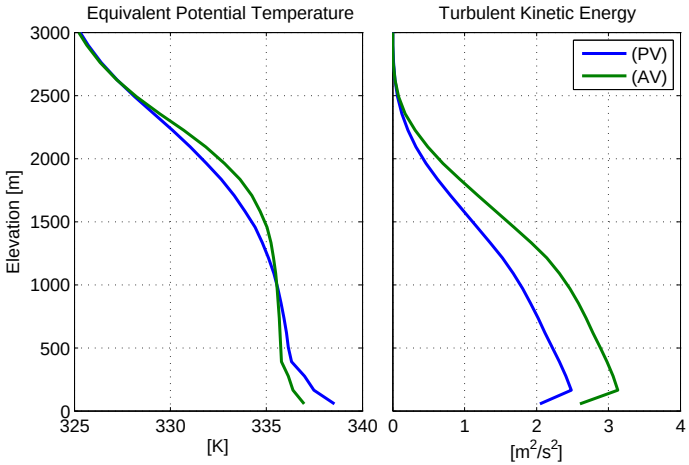

Fig. 7. Mean profiles of Equivalent Potential Temperature and Turbulent Kinetic Energy at 15Z (12 a.m. LT) within the bounded domain at Site 1.

HESSD
10, 15337–15373, 2013

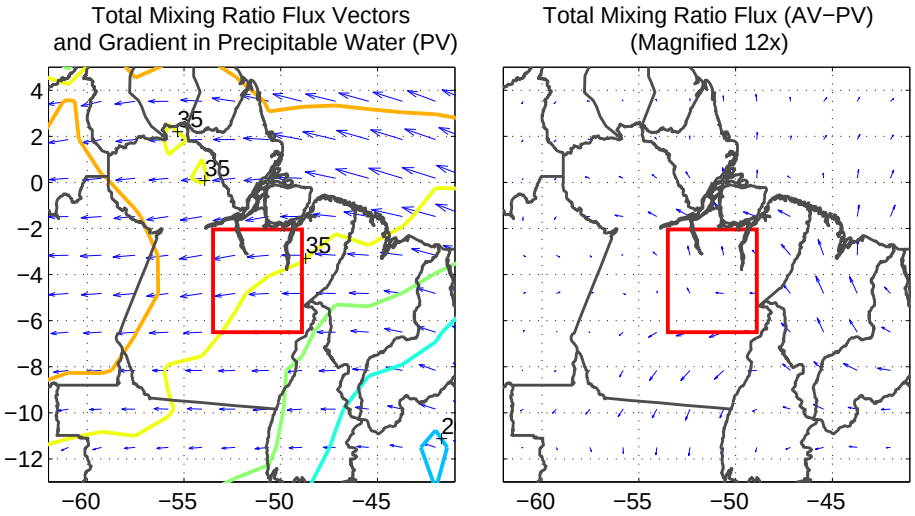

Fig. 8. Left panel: map of vertically integrated total water advective flux vectors (quivers) and vertically integrated precipitable water (contours) for the Actual Vegetation case (PV). September 2003. Quivers are scaled and convey only directionality and relative magnitude. Contours of low precipitable water are shown by cool colors (blues) and high precipitable water with warm colors (reds). Right panel: The differential in vertically integrated advection of total precipitable water, Potential Vegetation minus Actual Vegetation (AV–PV). Quivers are scaled to 12 times relative to the left panel.

HESSD
10, 15337–15373, 2013

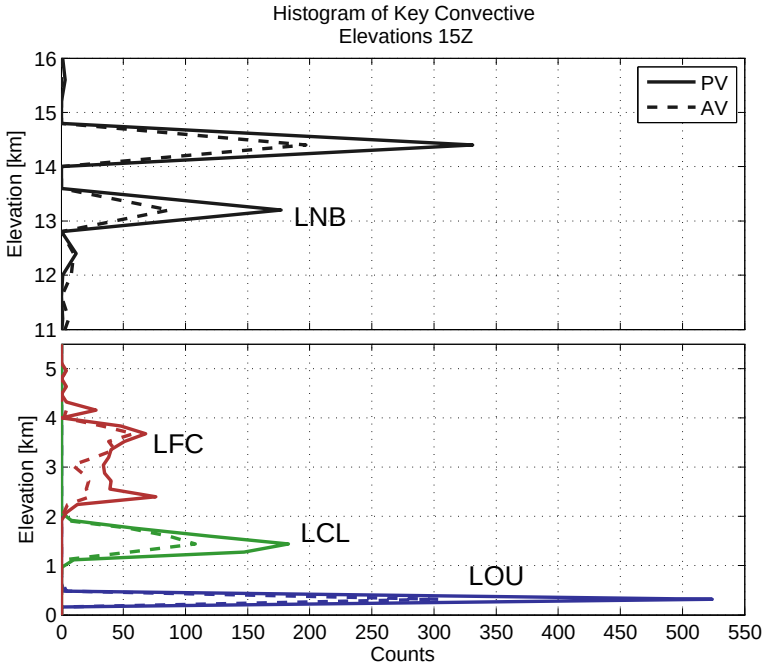

Fig. 9. Histograms for the elevations of key convective elevations at focus area 1 for successful convective events (ones that performed work and precipitation). LOU: Level of Updraft. LCL: Lifting Condensation Level. LFC: Level of Free Convection. LNB: Level of Neutral Buoyancy.

HESSD
10, 15337–15373, 2013

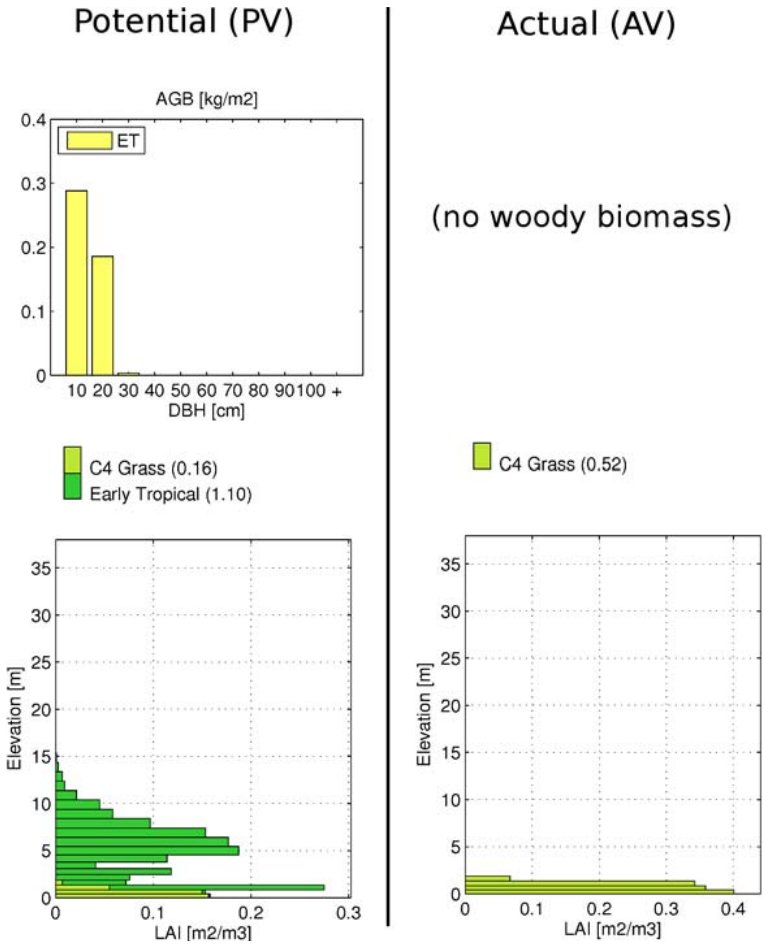

Fig. 10. Vegetation structure and composition estimated by the Ecosystem Demography Model 2 at Site 2 (19.5° S 63.5° W).

HESSD
10, 15337–15373, 2013

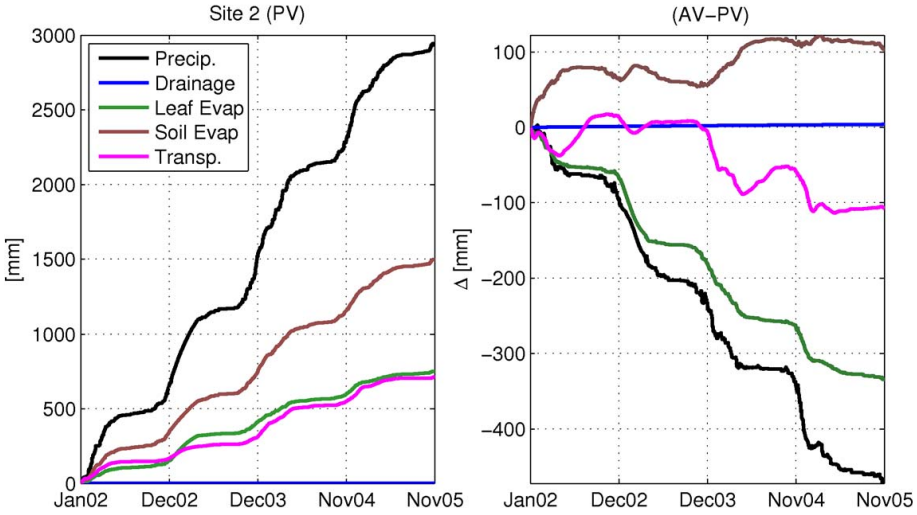

Fig. 11. Time series accumulations of water mass flux through the vegetation canopy at focus site 2 during the coupled model experiment, 2002–2005. The left panel shows accumulated fluxes in the PV case. Differences are shown in the right panel.

HESSD
10, 15337–15373, 2013

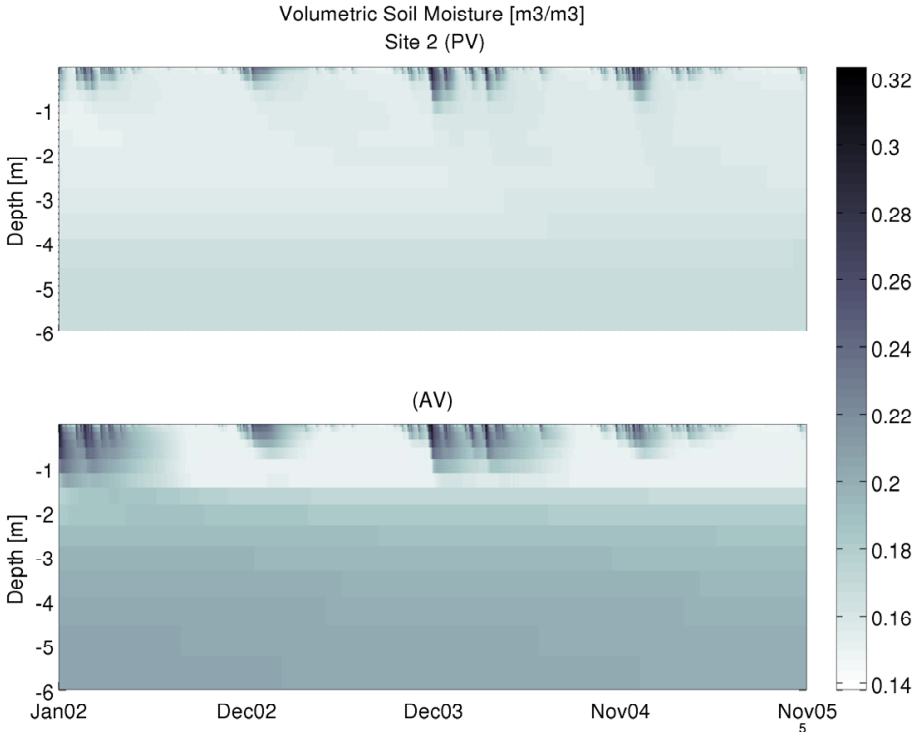

Fig. 12. Time series profile of volumetric soil water at focus site 2 (Chaco) during the coupled experiment. Both cases are shown.

HESSD
10, 15337–15373, 2013

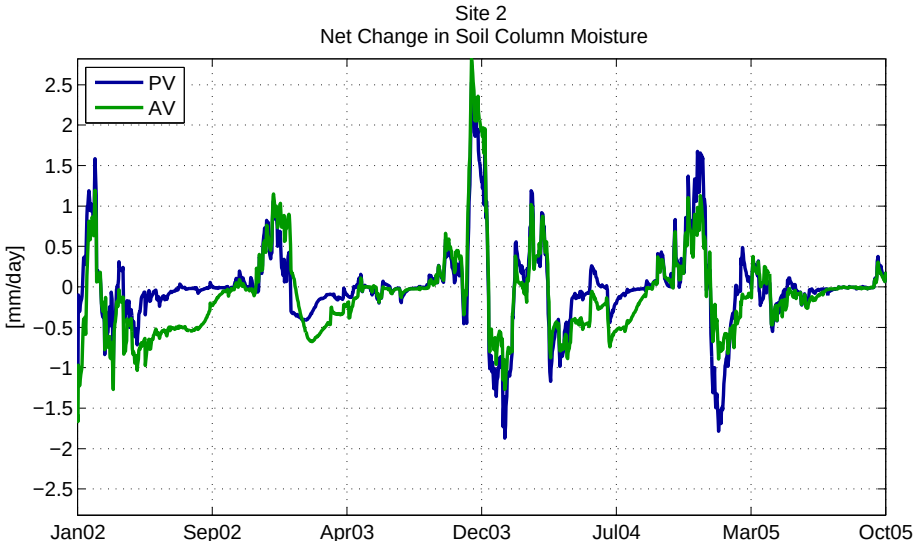

Fig. 13. Net rate of change in soil moisture at focus site 2, both conditions are shown. Positive values indicate the soil column is gaining water, negative values indicate the column is losing water. The intersection points of the time axis are good proxies as to the starts and stops of the dry season and wet season.

HESSD
10, 15337–15373, 2013

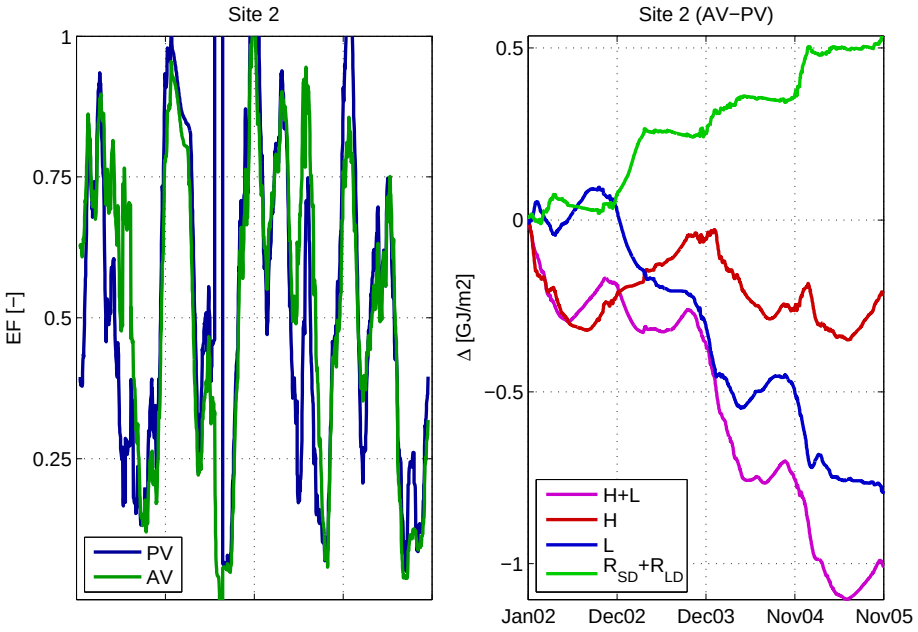

Fig. 14. Left panels: time series of evaporative fraction (latent/(latent+sensible)). Right panel: time series of the differential in accumulated energy fluxes. Site 2.

HESSD
10, 15337–15373, 2013

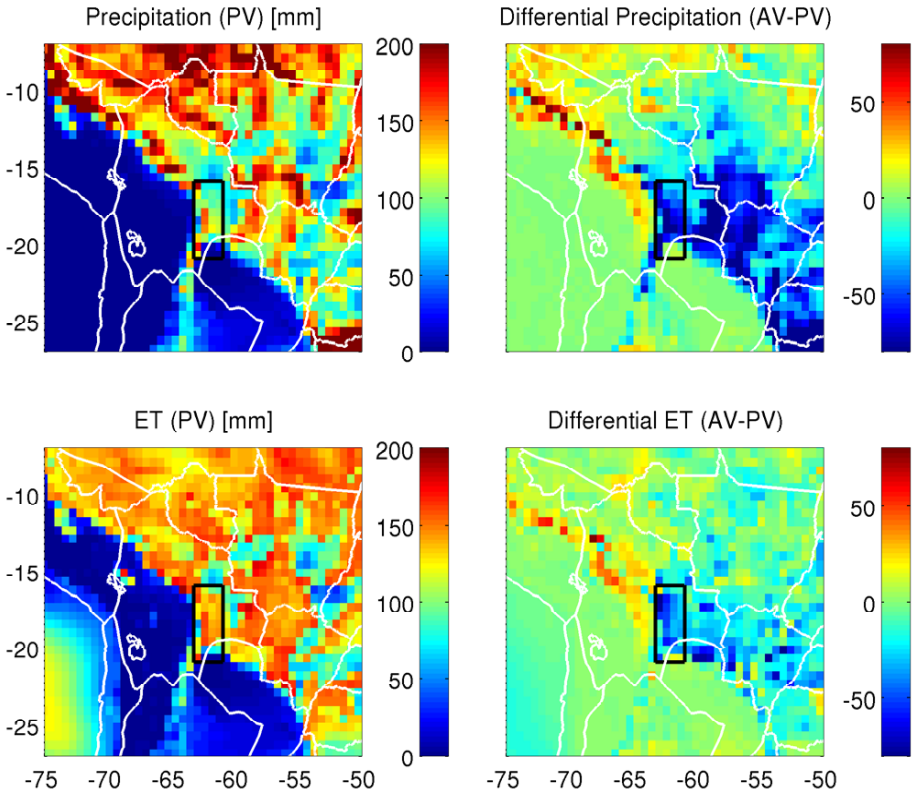

Fig. 15. Upper left panel: map of integrated monthly precipitation, case AV. Upper right panel: map of the integrated difference in monthly precipitation, case PV minus case AV. Lower right panel: map of integrated monthly evapotranspiration, case AV. Lower left panel: map of the integrated difference in monthly evapotranspiration, case PV minus case AV. The boundaries of the focus region are provided. April 2003.

HESSD
10, 15337–15373, 2013

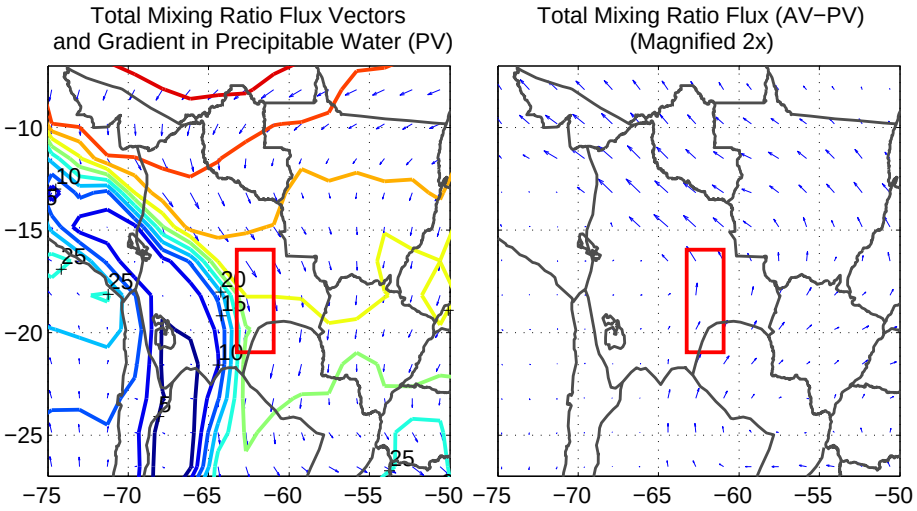

Fig. 16. Left panel: map of vertically integrated total water advective flux vectors (quivers) and vertically integrated precipitable water (contours) for the Actual Vegetation case (PV). September 2003. Quivers are scaled and convey only directionality and relative magnitude. Contours of low precipitable water are shown by cool colors (blues) and high precipitable water with warm colors (reds). Right panel: the differential in vertically integrated advection of total precipitable water, Potential Vegetation minus Actual Vegetation (AV–PV). Quivers are scaled to 20 times relative to the left panel.

HESSD
10, 15337–15373, 2013

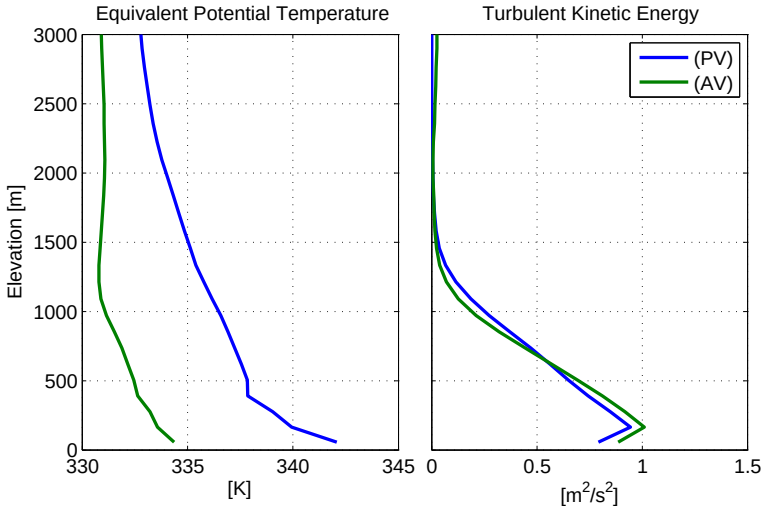

Fig. 17. Mean profiles of Equivalent Potential Temperature and Turbulent Kinetic Energy at 15Z (11 a.m. LT) within the bounded domain at Site 2.

HESSD
10, 15337–15373, 2013

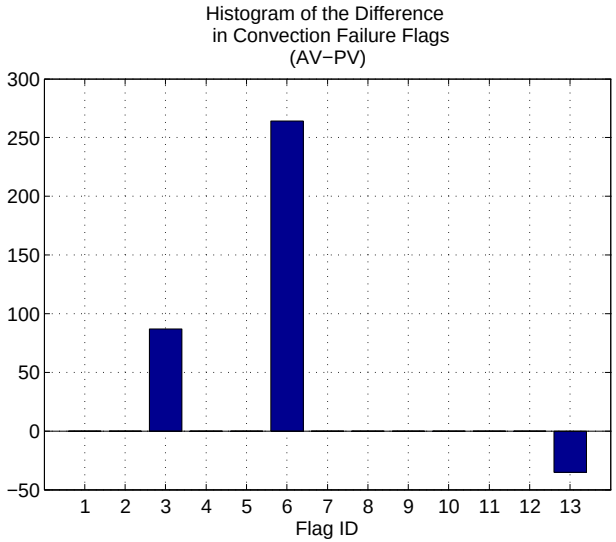

Fig. 18. Key: Flag 3: the level of free convection is too far from the level where updrafts originate, so it is out of reach. Flag 6: This cloud would be too thin to fall in this spectral type. Flag 13: dynamic control did not leave any positive member of reference mass flux, so this cloud can not exist.

HESSD
10, 15337–15373, 2013